JACS
JOURNAL OF THE AMERICAN CHEMICAL SOCIETY

Article

Unraveling the Crystallization Mechanism of CoAPO-5 Molecular Sieves under Hydrothermal Conditions

Didier Grandjean, Andrew M. Beale, Andrei V. Petukhov, and Bert M. Weckhuysen

J. Am. Chem. Soc., **2005**, 127 (41), 14454-14465• DOI: 10.1021/ja054014m • Publication Date (Web): 24 September 2005

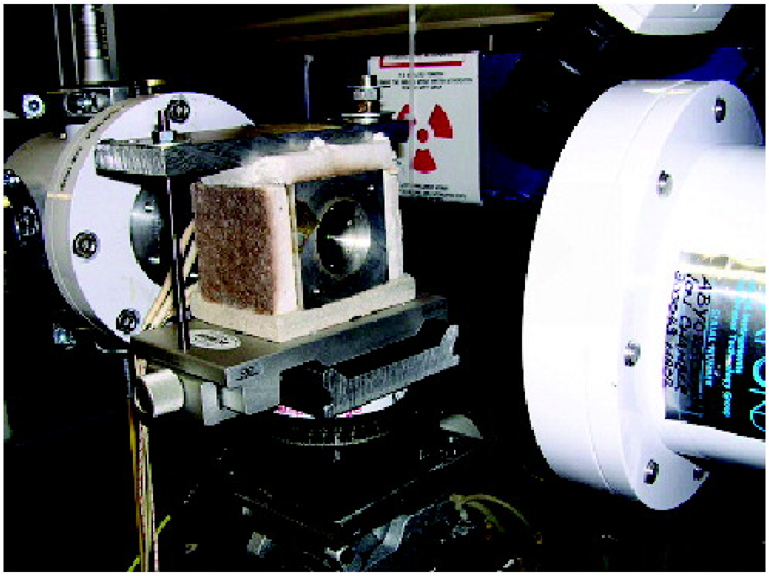

ACS Publications
High quality. High impact.

Journal of the American Chemical Society is published by the American Chemical Society. 1155 Sixteenth Street N.W., Washington, DC 20036

J|A|C|S
A R T I C L E S

Unraveling the Crystallization Mechanism of CoAPO-5 Molecular Sieves under Hydrothermal Conditions

Didier Grandjean,[†] Andrew M. Beale,[†] Andrei V. Petukhov,[‡] and
Bert M. Weckhuysen*,[†]

Contribution from the Department of Inorganic Chemistry and Catalysis, Debye Institute, Utrecht University, Sorbonnelaan 16, 3584 CA Utrecht, The Netherlands, and van't Hoff Laboratory for Physical and Colloid Chemistry, Debye Institute, Utrecht University, Padualaan 8, 3584 CH Utrecht, The Netherlands

Received June 17, 2005; E-mail: b.m.weckhuysen@chem.uu.nl

Abstract: The hydrothermal crystallization of CoAPO-5 molecular sieves has been studied using time-resolved in-situ SAXS/WAXS, UV−vis, Raman, and XAS. Data collected during heating to 180 °C allowed the observation of different steps occurring during the transformation of the amorphous gel into a crystalline material from a macroscopic and atomic perspective. Raman spectroscopy detected the initial formation of Al−O−P bonds, whereas SAXS showed that these gel particles had a broad size distribution ranging from ca. 7 to 20 nm before crystallization began. WAXS showed that this crystallization was sharp and occurred at around 160 °C. Analysis of the crystallization kinetics suggested a one-dimensional growth process. XAS showed that Co^{2+} transformed via a two-stage process during heating involving (i) a gradual transformation of octahedral coordination into tetrahedral coordination before the appearance of Bragg peaks corresponding to AFI, suggesting progressive incorporation of Co^{2+} into the poorly ordered Al−O−P network up to ca. 150 °C, and (ii) a rapid transformation of remaining octahedral Co^{2+} at the onset of crystallization. Co^{2+} was observed to retard crystallization of AFI but provided valuable information regarding the synthesis process by acting as an internal probe. A three-stage, one-dimensional crystallization mechanism is proposed: (i) an initial reaction between aluminum and phosphate units forming a primary amorphous phase, (ii) progressive condensation of linear Al−O−P chains forming a poorly ordered structure separated by template molecules up to ca. 155 °C, and (iii) rapid internal reorganization of the aluminophosphate network leading to crystallization of the AFI crystal structure.

1. Introduction

Understanding the principles that determine how porous crystalline materials such as zeolites and aluminophosphates are formed from a precursor gel under hydrothermal conditions is of considerable fundamental interest because it could lead to a more rational approach toward the design and synthesis of new molecular sieves.[1,2] Indeed, a great deal of research effort has been expended in an attempt to understand this phenomenon, and many conclusions and concepts have been proposed, most of which have been summarized in a recent review.[3] A very powerful but relatively unexplored way of probing these multicomponent heterogeneous processes is to perform in-situ studies of the crystallization in real time under real hydrothermal conditions, i.e., at elevated temperatures and pressures. A small number of in-situ studies of the crystallization of these materials have been performed using techniques such as electron paramagnetic resonance/electron−nuclear double resonance (EPR/ENDOR),[4,5] ultraviolet/visible spectroscopy (UV−vis),[6] nuclear magnetic resonance (NMR),[7−11] X-ray absorption spectroscopy (XAS),[12] X-ray diffraction (XRD),[13−17] small-angle neutron scattering (SANS),[18] and small-angle X-ray scattering (SAXS).[9,19−21] However, the application of one or two techniques to study in-situ crystallization means that the character-

---

[†] Department of Inorganic Chemistry and Catalysis.

[‡] van't Hoff Laboratory for Physical and Colloid Chemistry.

(1) Davis, M. E.; Lobo, R. F. *Chem. Mater.* **1992**, *4*, 756−768.
(2) Davis, M. E. *Nature* **2002**, *417*, 813−821.
(3) Cundy, C. S.; Cox, P. A. *Micropor. Mesopor. Mater.* **2005**, *82*, 1−78.
(4) Arieli, D.; Delabie, A.; Groothaert, M.; Pierloot, K.; Goldfarb, D. *J. Phys. Chem. B* **2002**, *106*, 9086−9097.
(5) Arieli, D.; Delabie, A.; Vaughan, D. E. W.; Strohmaier, K. G.; Goldfarb, D. *J. Phys. Chem. B* **2002**, *106*, 7509−7519.
(6) Weckhuysen, B. M.; Baetens, D.; Schoonheydt, R. A. *Angew. Chem. Int. Ed.* **2000**, *39*, 3419−3422.
(7) Vistad, O. B.; Akporiaye, D. E.; Taulelle, F.; Lillerud, K. P. *Chem. Mater.* **2003**, *15*, 1639−1649.
(8) Smaihi, M.; Barida, O.; Valtchev, V. *Eur. J. Inorg. Chem.* **2003**, 4370−4377.
(9) Houssin, C. J. Y.; Kirschhock, C. E. A.; Magusin, P.; Mojet, B. L.; Grobet, P. J.; Jacobs, P. A.; Martens, J. A.; van Santen, R. A. *Phys. Chem. Chem. Phys.* **2003**, *5*, 3518−3524.
(10) Burkett, S. L.; Davis, M. E. *J. Phys. Chem.* **1994**, *98*, 4647−4653.
(11) Burkett, S. L.; Davis, M. E. *Chem. Mater.* **1995**, *7*, 920−928.
(12) Sankar, G.; Thomas, J. M.; Rey, F.; Greaves, G. N. *J. Chem. Soc., Chem. Commun.* **1995**, 2549−2550.
(13) Rey, F.; Sankar, G.; Thomas, J. M.; Barrett, P. A.; Lewis, D. W.; Catlow, C. R. A.; Clark, S. M.; Greaves, G. N. *Chem. Mater.* **1995**, *7*, 1435−1436.
(14) Christensen, A. N.; Jensen, T. R.; Norby, P.; Hanson, J. C. *Chem. Mater.* **1998**, *10*, 1688−1693.
(15) Norby, P.; Christensen, A. N.; Hanson, J. C. *Inorg. Chem.* **1999**, *38*, 1216−1221.
(16) Norby, P.; Hanson, J. C. *Catal. Today* **1998**, *39*, 301−309.
(17) Muncaster, G.; Davies, A. T.; Sankar, G.; Catlow, C. R. A.; Thomas, J. M.; Colston, S. L.; Barnes, P.; Walton, R. I.; O'Hare, D. *Phys. Chem. Chem. Phys.* **2000**, *2*, 3523−3527.
(18) Watson, J. N.; Iton, L. E.; Keir, R. I.; Thomas, J. C.; Dowling, T. L.; White, J. W. *J. Phys. Chem. B* **1997**, *101*, 10094−10104.

10.1021/ja054014m CCC: $30.25

ization is often partial and unable to yield a full understanding of the crystallization behavior.

Of all of the techniques used perhaps XRD or wide-angle X-ray scattering (WAXS) is the most relevant to study the crystallization process and has been applied successfully to investigate the energetics and kinetics of crystallization as well as the identity of the intermediate crystalline phases during the synthesis of various zeolites and metalloaluminophosphates.[13,15,22] However, this technique is only sensitive to long-range order in the atomic size range and cannot provide information on the gel structure prior to the onset of crystallization. On the other hand, SAXS can unravel the number, dimension, shape, and organization of the small (nanometer-sized) scattering species present in the liquid/colloidal state before and during the crystallization process. The simultaneous measuring of the scattering of X-ray at small and wide angle is indeed a very powerful tool to correlate the formation and/or transformation of nanometer-scale structures with the onset of crystallization determined by the appearance of the first sign of the Bragg reflections of the crystalline phase in the WAXS pattern. De Moor et al. successfully applied these techniques to study organic-mediated zeolite crystallization from gelating and liquid systems.[21,23] They pointed out the presence of three categories of precursors in the gelating synthesis mixture before the onset of the crystallization: amorphous gel particles (600 nm), nanometer-scaled primary units, and aggregates composed of these units (10 nm). If the crystallization mechanism seemed to vary according to the structural type of the zeolite, primary units were found in all types of synthesis mixtures (gel or liquid) they investigated with a size varying from 2.8 to 1.5 nm according to the topology of the zeolite formed.[19] However, the shape (cylindrical or spherical)[18] and stoichiometry of these precursors remain unclear.

Aluminophosphate crystallization has received much less attention despite the closeness of their crystalline structures to those of zeolites.[3] A few studies have been reported in which attempts have been made to follow their crystallization, but only a handful of these were performed under in-situ conditions; therefore, the formation mechanism(s) is/are not well understood.[4,12,13,15−17,24] Little is known about their crystallization because it has rarely been studied using in-situ SAXS, with the study of Tiemann et al.[25] on mesostructured aluminophosphate/dodecyl phosphate composite materials being the only example found in the literature.

Investigation of the evolution of the local order around the individual atoms in the precursor gel before crystallization is also of great interest since it provides further insight into the crystallization process. In-situ time-resolved X-ray absorption spectroscopy is a particularly attractive technique for following the evolution of the local site environment of a selected element as a system undergoes nucleation and crystallization in structurally disordered or amorphous media.[26,27] However, XAS on materials such as molecular sieves containing only light atoms such as silicon, aluminum, and phosphorus is a rather difficult matter.[28] A convenient way to overcome this problem is to follow the structural and valence state evolution of a transition metal during the synthesis of microporous crystalline metalloaluminophosphate materials. Complementarily, this evolution can also be monitored by UV−vis spectroscopy.[6]

One of the more interesting and well-studied aluminophosphate structures is $AlPO_4$-5 (IZA code AFI).[29,30] The AFI structural type features a 12-ring one-dimensional hexagonal structure[30] and crystallizes rapidly with many different organic templates and a variety of incorporated heteroatoms and is therefore an ideal system for in-situ investigation.[6,12,13,31−33] In particular, introduction of Co^{2+} into the structure has been extensively investigated since it imparts catalytic function (such materials have been successfully employed in many catalytic reactions including production of olefins by dehydration of methanol,[34,35] aerobic selective oxidation of hydrocarbons[36−38]) to the material, and all studies agree that although in low levels Co^{2+} substitutes for Al^{3+} into the AlPO framework.[29] A preliminary in-situ combined QEXAFS/XRD study on CoAPO-5 has suggested that octahedral Co^{2+} ions in the precursor templated gel may become tetrahedrally coordinated prior to the onset of crystallization.[12] Because the changes affecting cobalt atoms during the crystallization of CoAPO-5 also reflect the changes affecting the gel, evaluation of the cobalt electronic state and local environment should provide valuable information on the mechanism of crystallization of this particular molecular sieve.[6]

We present here a combined in-situ study of the hydrothermal crystallization of CoAPO-5 starting from the precursor gel to the crystalline material using scattering techniques such as SAXS/WAXS as well as spectroscopic methods such as UV−vis, Raman, and XAS at the Co K-edge. This combined approach allowed us to achieve an understanding of the numerous interrelated processes taking place at both an atomic and a macroscopic level during the various stages of CoAPO-5 crystallization which are likely to be applicable to understanding the crystallization of other microporous materials.

2. Experimental Section

2.1. Gel Synthesis. The following chemicals were used in the synthesis: cobalt acetate tetrahydrate $C_4H_6CoO_4 \cdot 4H_2O$ (Acros Organics

---

(19) de Moor, P.; Beelen, T. P. M.; van Santen, R. A. *J. Phys. Chem. B* **1999**, *103*, 1639−1650.
(20) de Moor, P.; Beelen, T. P. M.; van Santen, R. A.; Beck, L. W.; Davis, M. E. *J. Phys. Chem. B* **2000**, *104*, 7600−7611.
(21) de Moor, P.; Beelen, T. P. M.; van Santen, R. A.; Tsuji, K.; Davis, M. E. *Chem. Mater.* **1999**, *11*, 36−43.
(22) Davies, A. T.; Sankar, G.; Catlow, C. R. A.; Clark, S. M. *J. Phys. Chem. B* **1997**, *101*, 10115−10120.
(23) de Moor, P.; Beelen, T. P. M.; Komanschek, B. U.; Beck, L. W.; Wagner, P.; Davis, M. E.; van Santen, R. A. *Chem.*−Eur. J. **1999**, *5*, 2083−2088.
(24) Loiseau, T.; Beitone, L.; Millange, F.; Taulelle, F.; O'Hare, D.; Ferey, G. *J. Phys. Chem. B* **2004**, *108*, 20020−20029.
(25) Tiemann, M.; Froba, M.; Rapp, G.; Funari, S. S. *Chem. Mater.* **2000**, *12*, 1342−1348.
(26) Clausen, B. S.; Topsoe, H.; Frahm, R. *Adv. Catal.*, **1998**, *42*, 315−344
(27) Cheetham, A. K.; Mellot, C. F. *Chem. Mater.* **1997**, *9*, 2269−2279.
(28) vanBokhoven, J. A.; Sambe, H.; Koningsberger, D. C.; Ramaker, D. E. *J. Phys. IV* **1997**, *7*, 835−840.
(29) Hartmann, M.; Kevan, L. *Chem. Rev.* **1999**, *99*, 635−663.
(30) Meier, W.; Olson, D. *Atlas of Zeolite Structure Types*, 3rd Revised ed.; Butterworth-Heinemann: Woburn, MA, 1992.
(31) Weckhuysen, B. M.; Rao, R. R.; Martens, J. A.; Schoonheydt, R. A. *Eur. J. Inorg. Chem.* **1999**, 565−577.
(32) Murugan, B.; Ramaswamy, V. In *Recent Advances in the Science and Technology of Zeolites and Related Materials, Parts A−C*; Stud. Surf. Sci. Catal. Vol. 154; Elsevier: Amsterdam, 2004; pp 971−977.
(33) Sanchez-Sanchez, M.; Sankar, G.; Simperler, A.; Bell, R. G.; Catlow, C. R. A.; Thomas, J. M. *Catal. Lett.* **2003**, *88*, 163−167.
(34) Chen, J. S.; Sankar, G.; Thomas, J. M.; Xu, R. R.; Greaves, G. N.; Waller, D. *Chem. Mater.* **1992**, *4*, 1373−1379.
(35) Franklin, I. L.; Beale, A. M.; Sankar, G. *Catal. Today* **2003**, *81*, 623−629.
(36) Schuchardt, U.; Cardoso, D.; Sercheli, R.; Pereira, R.; de Cruz, R. S.; Guerreiro, M. C.; Mandelli, D.; Spinace, E. V.; Fires, E. L. *Appl. Catal. A: Gen.* **2001**, *211*, 1−17.
(37) Thomas, J. M.; Raja, R.; Sankar, G.; Bell, R. G. *Acc. Chem. Res.* **2001**, *34*, 191−200.
(38) Moden, B.; Oliviero, L.; Dakka, J.; Santiesteban, J. G.; Iglesia, E. *J. Phys. Chem. B* **2004**, *108*, 5552−5563.

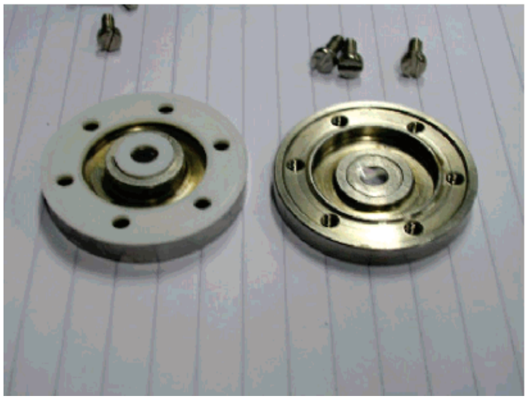

Figure 1. Cell used for all in-situ SAXS/WAXS, XAS, and UV−vis measurements.

99%), orthophosphoric acid H_3PO_4 (Acros Organics 85 wt % in water), triethylamine (TEA) (Acros Organics 99%), pseudoboehmite alumina CATAPAL B 73.6 wt % Al_2O_3 (Sasol North America Inc.). The precursor gels (pH $\approx$ 3.5) corresponding to the stoichiometry $Co_xAl_{1-x}PO_4$ with $x = 0.05$ (Co content $\approx$ 2.5 wt %) used, respectively, in the SAXS/WAXS and UV−Vis/XAS experiments were prepared by well-established methods before measurement.[34]

2.2. In-situ Synthesis Cell. In-situ XAS, SAXS/WAXS, and UV−vis measurements during crystallization were carried out in a cell described in Figure 1 made by assembling two circular pieces of stainless steel (45 mm diameter), each one fitted with a circular mica window (6 mm diameter) of ca. 30 μm thickness and separated by a Teflon ring (0.75 mm thick) and a Teflon spacer (1.5 mm thick). The bottom part of the tiny autoclave, delimited by the mica windows and the Teflon ring, was filled with the precursor gel up to a maximum of ca. 60% of its the total volume (ca. 2 mm^3) to avoid possible overpressure developing against the windows during the reaction. The cell was then heated in an insulated aluminum heating block controlled by a thermoregulator at a rate of 1°/min up to 180 °C and remained at this temperature for up to 3 h under autogenous pressure and static conditions. For easy comparison between the different experiments the reaction time t was scaled to the temperature T (1 °C = 1 min) with $t = 0$ min corresponding to $T = 0$ °C. Up to a value of 180 the time and temperature scale are identical, whereas values over 180 only correspond to reaction time given in minutes. In-situ Raman measurements were carried out in a quartz cell described elsewhere.[6]

2.3. SAXS/WAXS Measurements. Small- and wide-angle scattering data were collected on beamline DUBBLE (BM26B) at the European Synchrotron Radiation Facility (ESRF, Grenoble, France), operating at 6 GeV with a current of 200 mA. The beamline is equipped with a Si (111) double-crystal monochromator. SAXS patterns were measured at a wavelength of 1.00 Å using a gas-filled detector (130 × 130 mm^2) positioned at a distance of 1.5 m from the sample corresponding to scattering k vectors in the range $0.3 < k < 6$ nm^{-1}, which gave access to the first Bragg peak corresponding to the (100) reflection of the AFI structure (11.94 Å). Due to the very small amount of material formed during the reaction, the beam size was reduced to 300 × 300 μm and positioned at the lower part of the cell aperture. A gas-filled WAXS detector positioned at a distance of 20 cm was used to record the higher order Bragg reflections of the AFI crystalline structure. The high-intensity synchrotron radiation allowed us to collect SAXS and WAXS patterns simultaneously with a good signal-to-noise ratio every 2 min. The data were normalized for the intensity of the transmitted X-ray beam, thus correcting for the decay of the intensity as well as for sample absorption. Furthermore, a background subtraction was performed using data measured from a cell containing water. For the calibration of the SAXS and WAXS patterns a silver behanate[39,40] reference sample and a fully crystallized $AlPO_4$-5 material were used, respectively.

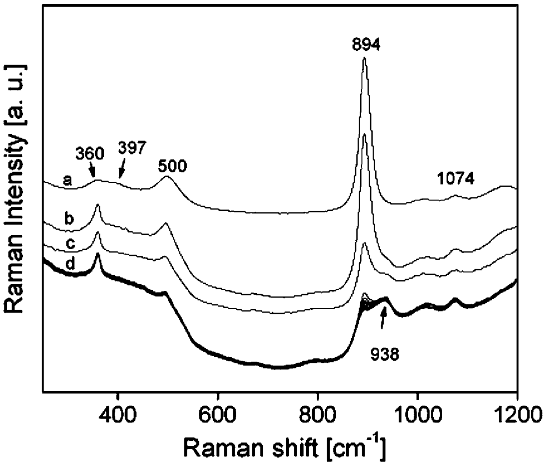

Figure 2. Raman spectra recorded at a time interval of 4 min after t_0 corresponding to the addition of H_3PO_4 to alumina dissolved in water: (a) $t = t_0$; (b) $t_0 + 4$ min; (c) $t_0 + 8$ min; (d) $t_0 + 12$ min to $t_0 + 76$ min. The two weak degenerate stretching (asymmetrical 1007 cm^{-1} and symmetrical 1050−1080 cm^{-1}) components of $P(OH)_3$ as well as a weak band at 1074 cm^{-1} corresponding to $H_2PO_4^-$ can also be observed in the spectra.

2.4. X-ray Absorption Spectroscopy. X-ray absorption data were collected on beamline DUBBLE (BM26A) at the European Synchrotron Radiation Facility (ESRF, Grenoble, France). This beamline is equipped with a Si (111) double-crystal monochromator. Quick EXAFS (QEXAFS) was measured in transmission mode with acquisition times of 3 min (4−250 ms acquisition time/point) with an energy resolution of 1.03 eV per point. Ionization chambers were filled with standard Ar/He mixtures. Data reduction of experimental X-ray absorption spectra was performed with the program EXBROOK.[41] Preedge background subtraction and normalization was carried out by fitting a linear polynomial to the preedge region and cubic splines to the postedge region of the absorption spectrum. EXAFS refinements were performed with the EXCURV98 package.[41] Phase shifts and backscattering factors were calculated ab initio using Hedin−Lundqvist potentials. Due to the relatively limited quality of the data, refinements were carried out using k^3 weighting typically in the range 3.5−8 Å^{-1}.

2.5. UV−vis DRS Spectroscopy. Diffuse reflectance UV−vis spectra were measured using a 600 μm optical fiber probe connected to both an Avantes AVS−SD2048 spectrometer and a halogen−deuterium light source. Multiple 50 ms spectra were collected over a period of 2.5 s every 2 min (the same time resolution as that used for SAXS/WAXS acquisition) during temperature ramping from 31 to 180 °C.

2.6. Raman Spectroscopy. Raman spectra were recorded with a Holoprobe Kaiser Optical spectrometer equipped with a holographic notch filter, CCD camera, and a 532 nm laser operating at 70 mW. During temperature ramping to 180 °C spectra were collected over a period of 30 s every 2 min (again the same time resolution as that used for SAXS/WAXS acquisition).

3. Results and Discussion

3.1. Raman Spectroscopy. The first stage of the gel preparation corresponding to reaction of the phosphoric acid with alumina has been monitored by Raman spectroscopy. Figure 2 shows the evolution of the Raman spectra at time intervals from 4 to 76 min after the phosphoric acid was added to the alumina/water mixture. Initially, the spectra are dominated

---

(39) Blanton, T. N.; Barnes, C. L.; Lelental, M. *J. Appl. Crystallogr.* **2000**, *33*, 172−173.
(40) Huang, T. C.; Toraya, H.; Blanton, T. N.; Wu, Y. *J. Appl. Crystallogr.* **1993**, *26*, 180−184.
(41) Binsted, N. C., Campbell, J. W.; Gurman, S. J.; Stephenson, P. C. *EXAFS Analysis Programs;* Daresbury Laboratory: Warrington 1991.

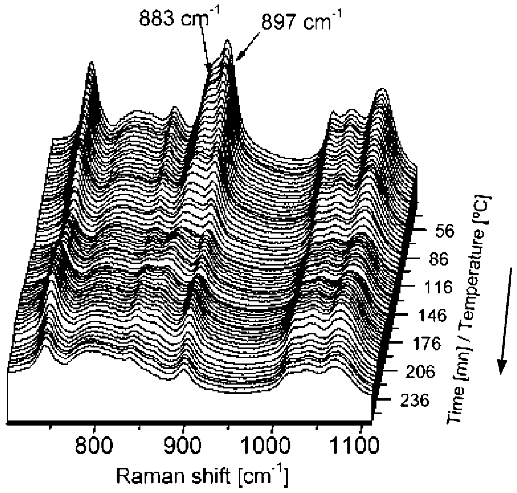

Figure 3. Stacked Raman spectra recorded in situ during crystallization of CoAPO-5 starting from the precursor gel. The two bands highlighted in the figure at 883 and 897 cm^{-1} are located at 920 and 909 cm^{-1}, respectively, in the unprotonated TEA template and can be assigned to asymmetrical bending in the plane of the C−H bond of the CH_3 group or stretching of the C−C bond.[50,51]

by a broad band at 500 cm^{-1} and two broad overlapping bands at 360 and 397 cm^{-1}, which correspond to the vibrational modes of isolated octahedral AlO_6 species.[42] However, 1−2 min after phosphoric acid addition the very intense peak at 894 cm^{-1} corresponding to the ν symmetrical stretching of $P(OH)_3$ characteristic of H_3PO_4 decreases dramatically in intensity and the ν stretching mode at 938 cm^{-1} for P−O bonds of $[PO_4]^{3-}$ tetrahedra starts to appear.[43] Furthermore, two sharp bands at 360 and 500 cm^{-1} corresponding to two δ Al−O−P vibrational modes can now be seen and are observed to increase with time. These results are consistent with the observations of Mortlock et al. that the phosphoric acid has already begun to react with the alumina to form Al−O−P units in the gel phase.[44,45]

Figure 3 presents a 3D-stacked plot of a selected region of the in-situ Raman spectra of the CoAPO-5 gel as a function of temperature. The bands present in the Raman spectra at the beginning of the in-situ crystallization experiment show a gradual diminution of intensity during heating although this is in part due to the increase in temperature.[42,43,46−49] With the exception of the bands at 360 and 494 cm^{-1}, all remaining bands of the CoAPO-5 precursor gel originate from the protonated TEA template.[42,43,46−49] It was observed that the 883 cm^{-1} band shifts with reaction time to values < 858 cm^{-1} almost as soon as the temperature increases, although it is difficult to follow up to its final stage since this peak overlaps with the 837 cm^{-1} band at the end of the reaction process. A high-pressure study carried out at 50 GPa of the TEA molecule[50] showed that, at this pressure, this band disappeared from the Raman spectrum, indicating that it is highly sensitive to the external conditions applied. The shift of this band in this work may reflect the increasing interaction of the template molecules with the Al−O−P units forming the gel. It is interesting to note that this interaction begins in the very early stage of the heating process.

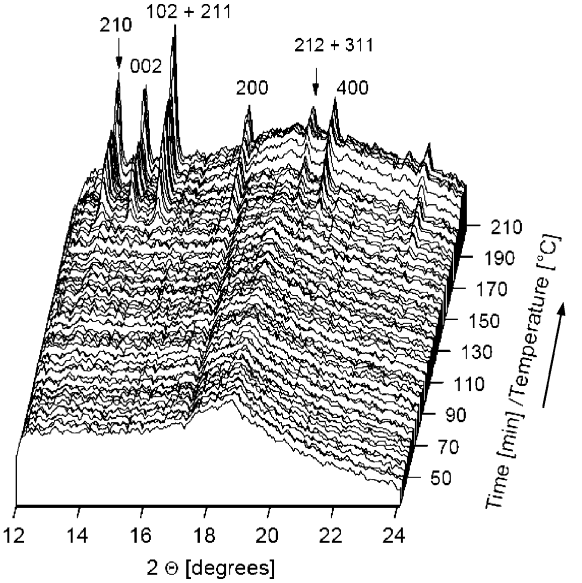

Figure 4. Three-dimensional stack plot of WAXS patterns recorded in situ during crystallization of CoAPO-5 starting from the precursor gel. The reflections can be indexed to the AFI structure.[52]

3.2. SAXS/WAXS. Figure 4 presents a three-dimensional stacked plot of a selected 2θ region of the wide-angle scattering pattern collected as a function of temperature during the transformation of the precursor gel into CoAPO-5. The onset of crystallization determined by the appearance of Bragg peaks in the pattern occurs at 160 °C. All reflections can be indexed using the AFI crystalline structure,[52] indicating that this phase forms exclusively. Moreover, it crystallizes directly from the amorphous precursor gel without the occurrence of any intermediate crystalline phase. The intensity of these peaks increased for approximately 40 min, after which no further change took place.

The evolution of diffraction peak intensity as a function of time can be used to derive valuable information on the kinetics and mechanism involved in the crystallization process. The intensity can be determined by fitting one or several Bragg peaks with a Gaussian function and measuring the corresponding areas that are then converted to the extent of reaction (α), scaled from 0 to 1, using the relationship $\alpha(t) = I_{hkl}(t)/I_{hkl}(\max)$, where $I_{hkl}(t)$ is the area of a given peak at time t and $I_{hkl}(\max)$ is the maximum area of this peak. Due to a better resolution of the SAXS detector, the first Bragg peak (100) corresponding to the largest d spacing value (11.94 Å) of the AFI structure was used to determine the extent of the reaction. The integration of this reflection is shown in Figure 5a, whereas the plot of the evolution of its full-width at half-maximum (fwhm) as a function of temperature is shown in Figure 5b.

The fwhm decreased very sharply up to a point that coincided approximately with the change in rate of the reaction observed

---

(42) Rudolph, W. W.; Mason, R.; Pye, C. C. *Phys. Chem. Chem. Phys.* **2000**, *2*, 5030−5040.

(43) Chapman, A.; Thirlwell, L. *Spectrosc. Acta* **1964**, *20*, 937

(44) Mortlock, R. F.; Bell, A. T.; Radke, C. J. *J. Phys. Chem.* **1993**, *97*, 767−774.

(45) Mortlock, R. F.; Bell, A. T.; Radke, C. J. *J. Phys. Chem.* **1993**, *97*, 775−782.

(46) Holmes, A. J.; Kirkby, S. J.; Ozin, G. A.; Young, D. *J. Phys. Chem.* **1994**, *98*, 4677−4682.

(47) Popescu, S. C.; Thomson, S.; Howe, R. F. *Phys. Chem. Chem. Phys.* **2001**, *3*, 111−118.

(48) Rokita, M.; Handke, M.; Mozgawa, W. *J. Mol. Struct.* **2000**, *555*, 351−356.

(49) Schnabel, K. H.; Finger, G.; Kornatowski, J.; Loffler, E.; Peuker, C.; Pilz, W. *Microporous Mater.* **1997**, *11*, 293−302.

(50) Gobin, C.; Marteau, P.; Petitet, J. P. *Spectrosc. Acta A* **2004**, *60*, 329−336.

(51) Takeuchi, H.; Kojima, T.; Egawa, T.; Konaka, S. *J. Phys. Chem.* **1992**, *96*, 4389−4396.

(52) Qiu, S.; Pang, W.; Kessler, H.; Guth, J. L. *Zeolites* **1989**, *9*, 440−444.

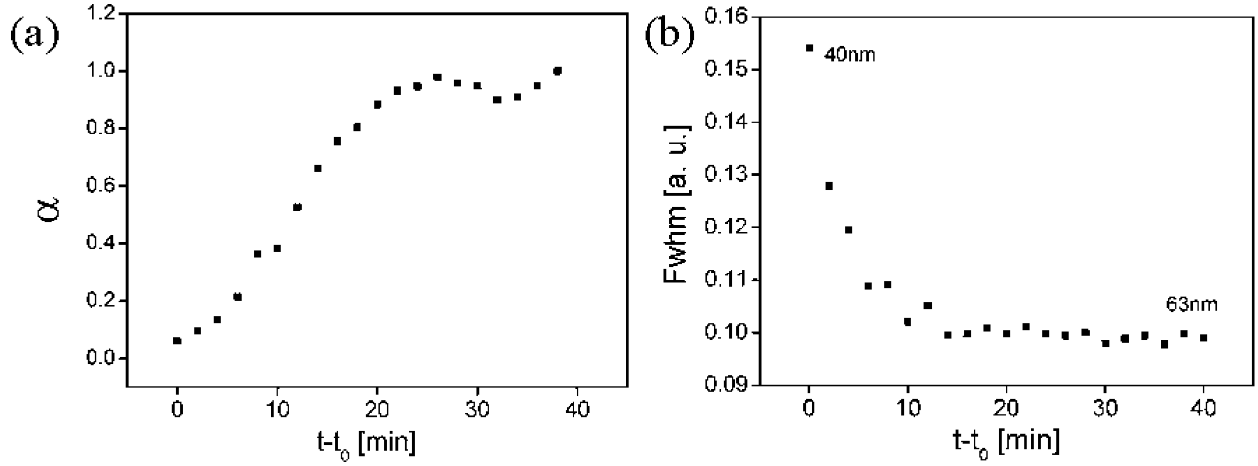

Figure 5. (a) Crystallization curve of CoAPO-5 with black squares representing the experimental integrated values of the (100) reflection as a function of time (t_0 corresponds to the onset of crystallization), and (b) evolution of the experimental full-width at half-maximum (fwhm) of the same reflection.

in Figure 5a. This remains effectively constant until the extent of the reaction reaches a maximum. This variation corresponds to an increase of the crystallites size from ca. 40 to 63 nm. Kinetic information on the crystallization process can be derived from the Avrami−Erofe'ev[53−56] expression that is widely used to model phase transitions and crystal growth in solid-state chemistry using the extent of the reaction, α, to time t using the relationship

$$\alpha = 1 - \exp[-(k(t - t_0))^n]$$

where t is the induction time, k the rate constant, and n the Avrami exponent. The exponent n can be used in most cases to deduce information about the rate of nucleation and the mechanism of nuclei growth. Common values of n range from $n = 0.5$ to 4 and contain information both on the dimensionality and the process of crystallization.[57] Previous work has demonstrated the relevance of this equation in modeling a variety of solid-state reactions but showed that this expression is found to be most applicable in the range $0.15 < \alpha < 0.8$.[58,59] A Sharp−Hancock plot ($\ln[-\ln(1 - \alpha)]$ vs ln(time)) has been used to obtain the gradient n and intercept $n \ln k$.[60,61] The resultant plot of the crystallization of CoAPO-5 presented in Figure 6 is clearly linear over the whole extent of the data, confirming the validity of the model (outliers due to the occurrence of macroscopic inhomogeneities in the sample during the synthesis were not included in the linear fitting process). The corresponding n and k parameters derived, respectively, from the gradient and intercept of the lines fitted by linear regression are $n = 1.50$ and $k = 6.55 \times 10^{-4}$ s^{-1}. These values can be compared to the corresponding values of $n = 1.02$ and $k = 2.00 \times 10^{-3}$ s^{-1} found for the crystallization of pure AlPO$_4$-5.[62] In other words, the k rate constant shows a nucleation rate 3 times slower in CoAPO-5 than in pure AlPO$_4$-5, indicating that the presence of cobalt significantly retards nuclei growth and crystallization. For CoAPO-5 the higher value of the n parameter of ca. 1.5 could indicate three possible mechanisms corresponding to (i) a 1D growth with a constant nucleation rate, (ii) a 1D growth phase boundary controlled, or, alternatively, (iii) a 2D growth with decreasing nucleation rate. However, it is generally understood that as n becomes larger, the rate of formation of nucleation sites becomes increasingly important in determining the overall rate of crystallization. A more plausible explanation in our case would be that CoAPO-5 crystallizes with the same 1D mechanism as pure AlPO$_4$-5 but that the presence of cobalt is slowing down the nucleation rate.

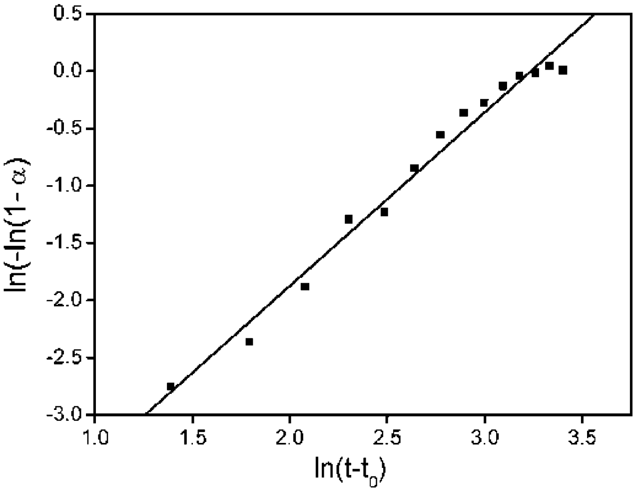

Figure 6. Sharp−Hancock plot for the formation of CoAPO-5 plotted data with $0.15 < \alpha < 0.8$.

The stacked 3D small-angle log-linear scattering profiles $I(k)$ measured in situ as a function of the crystallization temperature are shown in Figure 7a. The onset of crystallization can be easily observed by the appearance of the Bragg peak ($k = 5.26$ nm^{-1}) above 160 °C corresponding to the (100) reflection of the AFI structure, although no pronounced variations in the $I(k)$ profiles seem to occur at any stage of the crystallization process. However, it is clear that some significant variations of the scattering pattern appear more or less concomitantly with the occurrence of the AFI structure Bragg peak in the low k range (0.3−2 nm^{-1}). On the other hand, the relatively large fluctua-

---

(53) Erofe'ev, B. V. *C. R. Dokl. Acad. Sci. URSS* **1946**, *52*, 511−517.
(54) Avrami, M. *J. Chem. Phys.* **1939**, *7*, 1103.
(55) Avrami, M. *J. Chem. Phys.* **1940**, *8*, 212.
(56) Avrami, M. *J. Chem. Phys.* **1941**, *9*, 177.
(57) Hulbert, S. F. *J. Br. Ceram. Soc.* **1969**, *6*, 11−20.
(58) Fogg, A. M.; Price, S. J.; Francis, R. J.; O'Brien, S.; O'Hare, D. *J. Mater. Chem.* **2000**, *10*, 2355−2357.
(59) Beale, A. M.; Sankar, G. *Chem. Mater.* **2003**, *15*, 146−153.
(60) Hancock, J. H.; Sharp, J. D. *J. Am. Ceram. Soc.* **1972**, *55*, 74−77.
(61) Milanesio, M.; Artioli, G.; Gualtieri, A. F.; Palin, L.; Lamberti, C. *J. Am. Chem. Soc.* **2003**, *125*, 14549−14558.
(62) Grandjean, D.; Beale, A. M.; Petukhov, A. V.; Weckhuysen, B. M. Manuscript in preparation.

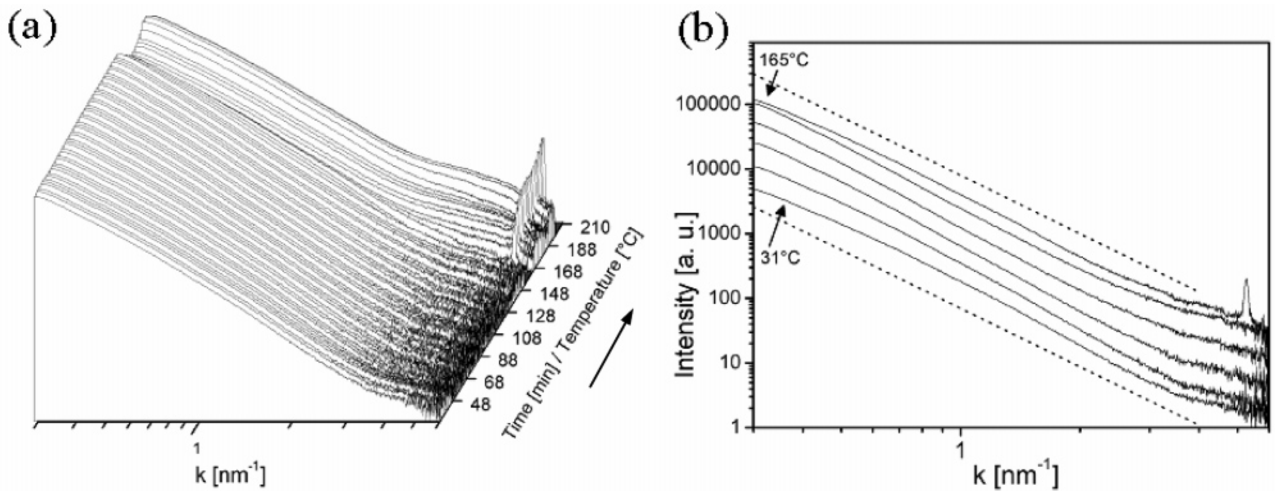

Figure 7. (a) Three-dimensional stack log−log plot of SAXS patterns recorded in situ during crystallization of CoAPO-5 starting from the precursor gel. (b) A few selected $I(k)$ profiles before and one after crystallization in log−log representation. The curves are displaced for clarity. The dashed lines illustrate the q^{-3} decay. The curves correspond (bottom to top) to temperatures of 31, 71, 111, 151, and 165 °C.

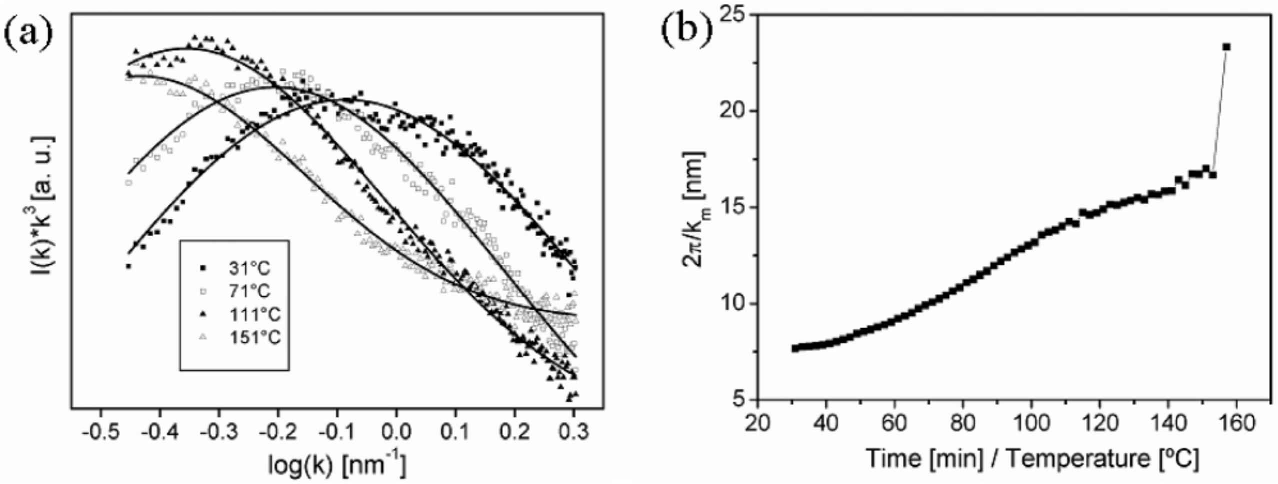

Figure 8. (a) Selected $I(k)k^3 - \log(k)$ plots corresponding to temperatures of 31, 71, 111, and 151 °C. A few selected examples of the SAXS data reploted in $I(k)k^3$ versus $\log(k)$ coordinates. The smooth curves are the results of Gaussian fits. (b) Evolution of $2\pi/k_{\max}$ maximum as a function of temperature during crystallization of CoAPO-5.

tions of the SAXS intensity that clearly appear after the onset of crystallization are more probably related to macroscopic movements of the reaction products within the synthesis cell leading to fluctuations of the content of the volume irradiated with the X-ray beam than to real structural changes. Contrary to the work of de Moor et al.[20,21] carried out on zeolites, no marked feature in the scattering pattern that could be directly linked to the existence of clear primary units was visible in our work.

A clearer view of the changes affecting the scattering profile as a function of temperature is presented in Figure 7b, which shows a limited selection of five log−log $I(k)$ scattering profiles measured at various temperatures before the onset of crystallization as well as one profile taken above it. The SAXS intensity $I(k)$ closely follows a power-law decay k^{-n} with n close to −3 as shown in Figure 7b. This decay is slower than the asymptotic behavior of $I(k)$ with $n = -4$ predicted by the Porod law for compact particles with sharp interfaces, indicating that this system has a more complex multiscale structure. Very similar decay of the scattering intensity has already been observed in various SAXS studies conducted on the crystallization of different types of zeolites, suggesting that such a spectrum of spatial density fluctuations is common to the precursor gel phase for molecular sieves.[20,21]

Despite the apparent similarity between the profiles presented in Figure 7b, a detailed analysis shows that small variations can be detected during the various stages of the reaction. By focusing on the k range from 0.35 to 2 nm^{-1} and removing the leading k^{-3} decay by plotting the $I(k)k^3$ dependences it is possible to observe a difference between the scattering profiles of Figure 7b as shown in Figure 8. Indeed, all the re-plotted profiles show a broad maximum which monotonically shifts to smaller k values with increasing temperature, apparently up to the onset of crystallization. We fitted the obtained $k^3I(k)$ dependences versus $\log(k)$ to Gaussian profiles, which are also illustrated in Figure 8. Although the choice of the Gaussian function is rather arbitrary since any other bell-shaped function could be used, it is able to yield a sufficiently good fit of the data when the temperature is not too high. In the following we will only focus on the data corresponding to the lower temperatures. From the Gaussian fits we have determined the values $k_{\max}$ corresponding to the maximum of the $I(k)k^3$ dependence. The corresponding reciprocal values $2\pi/k_{\max}$ for all scattering profiles measured during the crystallization process

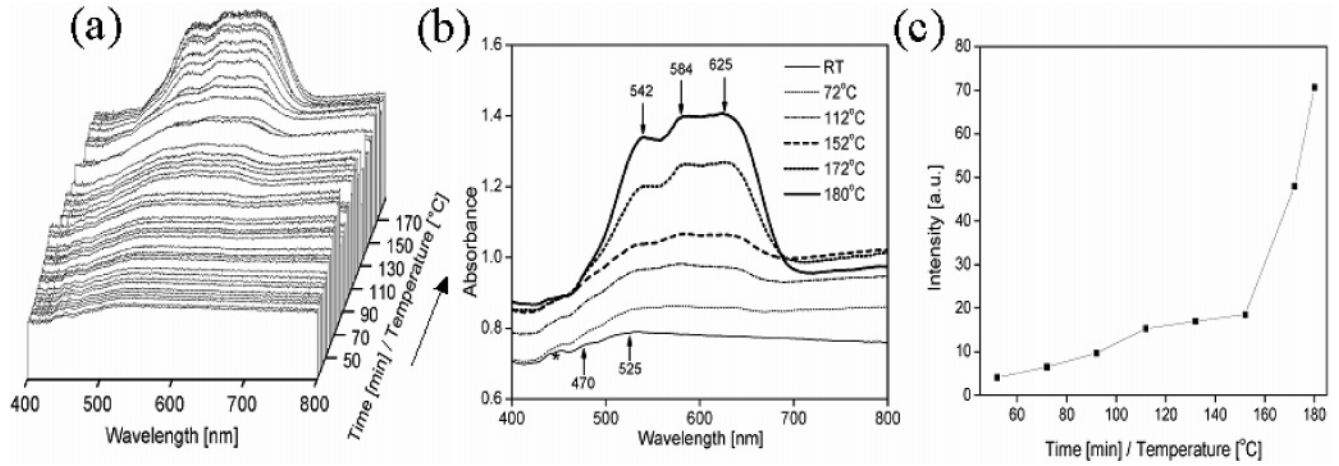

Figure 9. (a) Stacked UV−vis spectra recorded in situ during crystallization of CoAPO-5 starting from the precursor gel, and (b) a selected few of these UV−vis spectra. (c) Evolution of the integrated intensity of the triplet corresponding to pseudo-tetrahedral Co^{2+} as a function of temperature.

are plotted as a function of temperature in Figure 8b. Surprisingly, these values display very little noise despite of the significant uncertainties of the original data. The results show a very different behavior before and after crystallization. As the temperature increases from 30 to 150 °C, $2\pi/k_{max}$ undergoes a smooth and monotonic increase. At 160 °C the presence of the Bragg peak changes the shape of the $I(k)k^3$ dependence. The values of k_{max} yielded by the fit quickly increase to much larger k values due to an increase of the scattering intensity at $k > 2$ nm^{-1}. This increase might be related to formation of amorphous structures. However, instabilities of the scattering intensity at $T > 160$ °C induced by strong convection of the reaction products prevent us from making quantitative conclusions.

Although the data does not provide us with sufficient evidence of the exact nature of the structural transformation in the gel, it is tempting to assign the position of the maxima in $k^3I(k)$ dependence to a specific physical scale in the system, such as, for example, the inverse of the typical size of the gel aggregates that are precursors of the AFI crystallites. Such an interpretation is supported by the fact that the final size of about 20 nm found at the onset of crystallization is on the order of the crystallite size (40 nm) determined from the width (fwhm) of the Bragg peak, suggesting that this physical scale as determined with SAXS analysis may correspond to particles possessing a higher level of order than the surrounding gel. However, the very broad nature of the Gaussian fits suggests that the size distribution of these aggregates is very large and that k_{max} corresponds only to the center of the distribution curve. The size of these particles monotonically increases as a function of temperature from ca.7 nm at room temperature up to ca. 20 nm just before the onset of crystallization by successive additions of low-order Al−O−P units, possibly chains, from the gel. This process already started at temperatures as low as about 40 °C, and at 160 °C the particles eventually crystallize forming the AFI structure.

3.3. UV−vis Spectroscopy. Evolution of the Co^{2+} coordination during crystallization has been monitored also by UV−vis spectroscopy. Figure 9 shows the 3D-stacked DRS spectra of the in situ crystallization plotted as a function of time and a selection of the DRS spectra at different reaction temperatures. The spectrum of the pink precursor gel measured at room temperature contains two bands located at 525 and 470 nm (appreciable in part b only) which correspond to the $^4T_{1g}$ (F) → $^4T_{1g}$ (P) transition (ν_3 band) of high-spin Co^{2+} hexahydrate $[Co(H_2O)_6]^{2+}$ and the $^4T_{1g}$ (F) → $^4A_{2g}$ (P) (ν_3 band) of high-spin Co^{2+} species of the type $[CoO_4(H_2O)_2]^{2+}$ or $[CoO_5(H_2O)]^{2+}$, respectively.[6] The last two types of species are thought to be connected via phosphate groups of the AlPO species in the precrystalline gel. As the temperature increased, a triplet, with absorption bands at 542, 584, and 625 nm assigned to the $^4A_{2g}$ (F) → $^4T_1$ (P) transition (ν_3 band) of high-spin pseudo-tetrahedral Co^{2+} becomes evident in the spectra, suggesting a gradual conversion from octahedral to tetrahedral coordination. A plot of the integrated area of this triplet plotted as a function of temperature in Figure 9c shows qualitatively that this might be a two-stage conversion process, relatively slow up to a temperature of ca. 150 °C, but much quicker above this. This indicates that the Co^{2+} transformation from octahedral into tetrahedral coordination is occurring throughout the whole heating process, slowly in a first stage and much more rapidly just before/during crystallization. However, a change in density of the sample as a consequence of crystallization may also cause an increase in absorption above 155 °C. To determine further whether Co^{2+} coordination changes before crystallization begins, XAS measurements were performed.

3.4. XAS (XANES and EXAFS). As in most of the transition metals, the Co^{2+} spectrum features a preedge located at ca. 7710 eV due to the 1s 3d−e_g transition.[63] Although this is dipole forbidden in an ideal centrosymmetric octahedral symmetry, the appearance of the weak absorption is due to pure electric quadrupole coupling and the noncentrosymmetric environment of the slightly distorted CoO_6 octahedral geometry. The intensity of this preedge is very sensitive to the cobalt environment and increases significantly when the coordination changes from centrosymmetric to noncentrosymmetric. The white line in the XANES spectra corresponds to an electric dipole-allowed transition of a 1s−4p bound state with T_{1u} symmetry.[64]

Figure 10a shows a stackplot of background-subtracted and normalized XANES spectra recorded during crystallization as a function of time, whereas the simultaneous variation of the integrated intensity of the preedge feature is presented in Figure 10b. Two regions can clearly be identified in both plots. The first encompasses the beginning of the synthesis up to ca. 150

---

(63) Barrett, P. A.; Sankar, G.; Catlow, C. R. A.; Thomas, J. M. *J. Phys. Chem.* **1996**, *100*, 8977−8985.

(64) Buffat, B.; Tuilier, M. H. *Solid State Commun.* **1987**, *64*, 401−406.

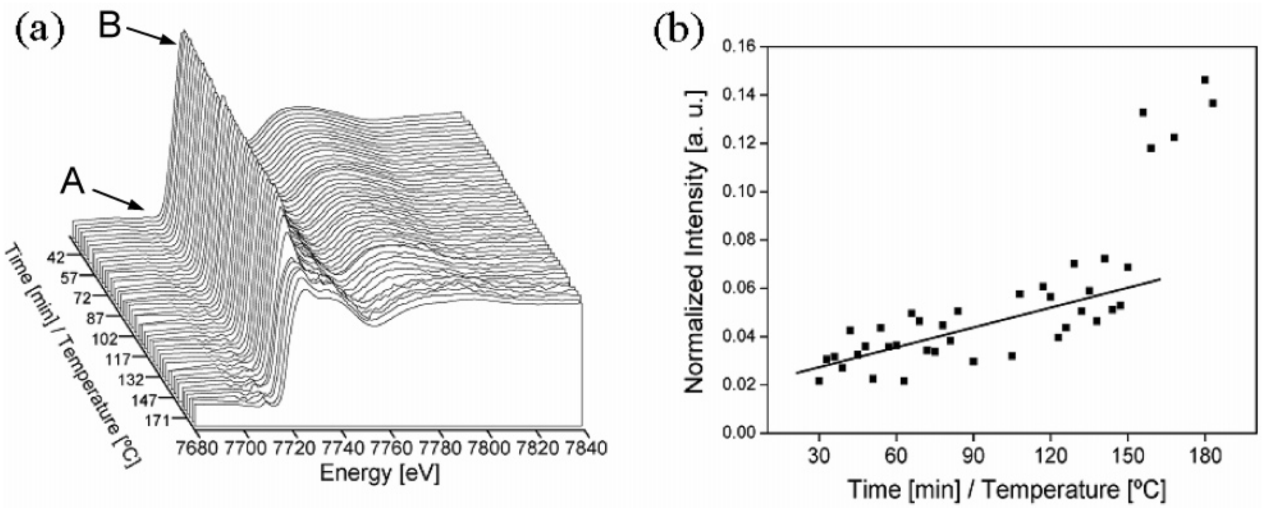

Figure 10. (a)Three-dimensional stack plot of background-subtracted and normalized XANES spectra at the Co K-edge recorded in situ during crystallization of CoAPO-5 starting from the precursor gel. The features labeled A and B correspond to the preedge peak (1s−3d transition) and white line (1s−4p transition), respectively. (b) Evolution of the integrated intensity of the preedge feature A as a function of crystallization time. Although not shown here, the white line feature B also changes with crystallization time, although the trend is opposite to that seen for the preedge feature. The increase in the preedge intensity and decrease in white line shows that the original octahedral geometry of cobalt coordination loses its centrosymmetric character in a two-step process.

°C, which is characterized by a slow monotonic decrease in white line intensity, an increase in the normalized preedge intensity from 0.03 to ca. 0.07, and a shift in the position of the first oscillation toward higher energies. The second region encompasses the trends observed in the first region occurring much more rapidly (the intensity of the preedge peak almost doubled to 0.13 in less than 10 min) before stabilizing for the remainder of the reaction. These changes indicate that reduction in the average Co−O coordination and bond distances has occurred and is consistent with a change in the cobalt coordination from octahedral to tetrahedral rather than a simple distortion of the octahedral coordination or the highly improbable occurrence of a 5-fold coordination. This was strongly supported by the UV−vis data that clearly showed the amount of tetrahedral Co^{2+} increasing in a two-step mode from the very early stage of the heating process to the final crystallization of the AFI material. We note that there is no significant change in edge energy at 7719.3 eV or the position of the preedge feature at ca. 7110 eV, which would suggest that no appreciable change in the cobalt oxidation state occurs during the crystallization process.[65,66] However, it is known that Co^{2+} oxidation to Co^{3+} does not occur readily in CoAPO-5 materials.[63,67]

Figure 11a contains a stacked 3D plot of the Fourier transforms of the Co K-edge EXAS as a function of time. It is clear that the cobalt environment changes during crystallization in a more complex way than the XANES analysis suggested. On heating from room temperature to ca. 100 °C, two broad peaks can be seen: the first intense peak corresponds to the first coordination shell of oxygen (ca. 2.08 Å), whereas the second can be fitted to a shell of phosphorus (ca. 3.20 Å). The intensity and position of these two peaks do not vary significantly during this time, indicating that the environment of cobalt is relatively stable in the early stages of the reaction. During the second stage from 100 to 156 °C the main peak shows a constant decrease in its intensity associated with a constant shift toward smaller *R* values (from ca. 2.08 toward 2.02 Å), whereas the second peak (ca. 3.20 Å) becomes much sharper. At the same time two new peaks of weak intensity at higher *R* values (ca. 4.00 and 5.00 Å) are appearing, suggesting that the building up of long-range order around the cobalt atoms has begun. These peaks again seem to reduce in intensity between 135 and 160 °C, suggesting that the disorder around the cobalt species increases further just before crystallization. This, however, may also be a consequence of lower data quality at this stage of the reaction since changes in the density of the gel results in differing amounts of material being ‘seen’ by the beam positioned at the lower part of the cell. At 160 °C the first peak gains intensity and begins to shift toward a lower *R* value (from 2.02 to 1.94 Å) and the second and third peaks (ca. 4.00 and 5.00 Å) became both sharper and more intense. These changes coincide with the onset of crystallization determined by the occurrence of the Bragg peaks of the AFI structure in both the WAXS and the SAXS pattern. The last two FT corresponding to the EXAS measured 2 h after the onset of crystallization show that surprisingly the cobalt environment in the crystalline phase has changed further. The peaks are slightly broader, indicating the presence a higher disorder in the cobalt environment, and their position is shifted to higher *R* values.

Figure 11b presents the detailed evolution of the Co−O bond length of the first coordination shell as a function of temperature. As the UV−vis and XANES analysis indicated, two different regions can be identified in this plot. A first region from the start of heating to 150 °C followed by a shorter one up to 180 °C. Initially up to ca. 75 °C the Co−O bond distance remains relatively stable around 2.08 Å, but beyond this temperature a long and regular shortening of the Co−O bond length to 2.04 Å occurs as a linear function of temperature. In the second region this shortening is sudden and more rapid with the distance

---

(65) Lamberti, C.; Prestipino, C.; Bonino, F.; Capello, L.; Bordiga, S.; Spoto, G.; Zecchina, A.; Moreno, S. D.; Cremaschi, B.; Garilli, M.; Marsella, A.; Carmello, D.; Vidotto, S.; Leofanti, G. *Angew. Chem., Int. Ed.* **2002**, *41*, 2341−2344.

(66) Lamberti, C.; Bordiga, S.; Bonino, F.; Prestipino, C.; Berlier, G.; Capello, L.; D'Acapito, F.; Xamena, F.; Zecchina, A. *Phys. Chem. Chem. Phys.* **2003**, *5*, 4502−4509.

(67) Beale, A. M.; Sankar, G.; Catlow, C. R. A.; Anderson, P. A.; Green, T. L. *Phys. Chem. Chem. Phys.* **2005**, *7*, 1856−1860.

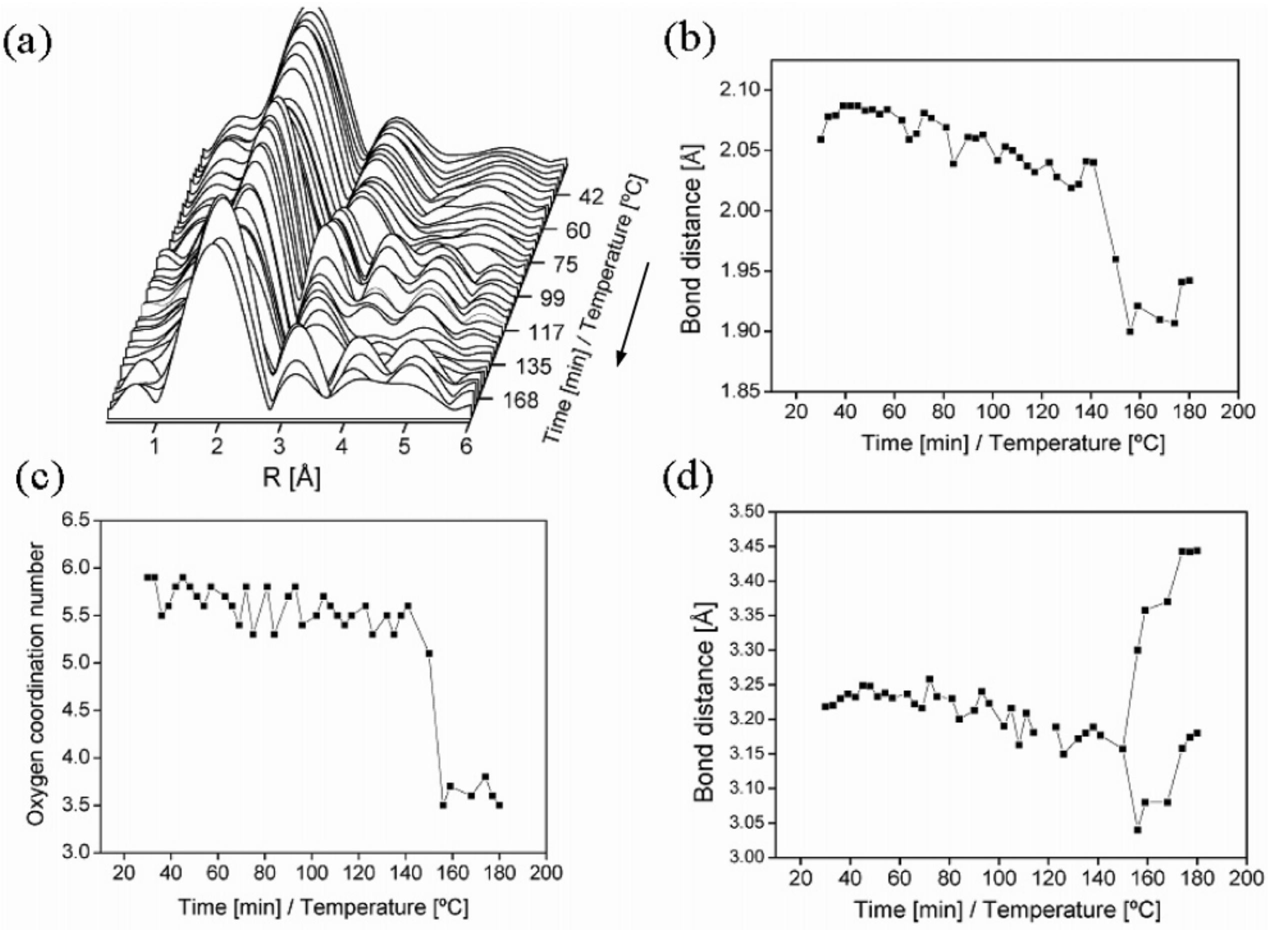

Figure 11. (a) Three-dimensional stack plot of the Fourier transforms of EXAS data (k^3 weighted over a k range from 3.5 to 8 Å^{-1}) recorded in situ at the Co K-edge during crystallization of CoAPO-5 starting from the precursor gel. (b and c) Evolution of the cobalt−oxygen bond distance and coordination number; (d) evolution of cobalt−phosphorus bond distances corresponding to the second and third coordination shells as a function of crystallization temperature.

dropping in less than 15 min from 2.04 to 1.90 Å before increasing after 2 h to 1.94 Å corresponding to the typical distance of tetrahedral Co−O in the final CoAPO-5 material.[63] Although the Co−O coordination number cannot be determined with a very high accuracy due to the limited quality of the data, evolution of the oxygen coordination number as a function of temperature (Figure 11c) confirms the general two-stage evolution of the Co−O bond distances with the first oxygen shell coordination number slowly decreasing from ca. 5.9 to 5.1 from room temperature to ca. 150 °C and suddenly dropping to ca. 3.6 (we note that the expected coordination number at this stage should be 4.0, although due to the difficulty of obtaining high data quality in such experiments we estimate that the error in determining coordination numbers at this stage is likely to be much higher than normal) at ca.156 °C and in the final material.

The behavior of the phosphorus coordination shells mirrors that of the first oxygen shell. Figure 11d shows that the first region corresponds to a single phosphorus shell with a Co−P bond distance decreasing slowly from ca. 3.24 Å at the beginning of the reaction to 3.18 Å at 145 °C and a coordination number increasing accordingly from ca. 1 to 2. In the second stage of the reaction two bond distances corresponding each to ca. two phosphorus atoms can be identified varying, respectively, from 3.04 and 3.30 Å at ca. 156 °C to 3.18 and 3.44 Å in the final material.

Despite a certain lack of accuracy of the first shell oxygen coordination numbers it is possible to characterize the geometry of the Co^{2+} species in a reliable way using the information provided by the average Co−O distance that is determined with a much better precision. Indeed, typical Co−O bond distances of 2.08 and 1.95 Å generally characterize, respectively, the octahedral and tetrahedral coordination, the two stable geometries adopted by Co^{2+} species.[68] It is clear that until the reaction temperature reaches 75 °C, Co^{2+} is in octahedral coordination, existing as Co^{2+} hexaaqua-like species in the precursor gel since the Co−O bond distance is stable around 2.08 Å. However, these hydrated species are not entirely free since the cobalt is forming a single Co−O−P bond with the Al−O−P units as shown by the presence of a single phosphorus atom in the EXAFS data at a distance of 3.24 Å. The occurrence of such species has been postulated previously and is thought to be responsible for the band at 470 nm in the UV−vis. Above this temperature the Co−O and Co−P bond distances shorten to 2.04 and 3.18 Å, respectively (the phosphorus coordination number also increases to 2). This shortening seems to reflect a gradual transformation of octahedral Co^{2+} into tetrahedral species as a function of the reaction time and their concomitant incorporation in the Al−O−P network. If we consider that octahedral Co^{2+} is coordinated to six oxygens at 2.08 Å and that tetrahedral Co^{2+} is coordinated to four oxygens at 1.95 Å, the relative amounts δ_{CoOh} and $\delta_{\mathrm{Co}}\mathrm{T}_{\mathrm{d}}$ of the two species can be evaluated using the Co−O bond distance $R_{\mathrm{Co-O}}$ determined from

---

(68) Fletcher, D. A.; McMeeking, R. F.; Parkin, D. *J. Chem. Inf. Comput. Sci.* **1996**, *36*, 746−749.

EXAFS and weighted by the respective coordination number of the two cobalt species.[63,68] Solving the equations $R_{\mathrm{Co-O}} = 6 \times 2.08 \times \delta_{\mathrm{CoOh}} + 4 \times 1.95 \times \delta_{\mathrm{Co}}\mathrm{T_d}/(6 \times \delta_{\mathrm{CoOh}} + 4 \times \delta_{\mathrm{Co}}\mathrm{T_d})$ and $\delta_{\mathrm{CoOh}} + \delta_{\mathrm{Co}}\mathrm{T_d} = 100$ gives a ratio of $\delta_{\mathrm{Co}}\mathrm{T_d} = 57\%$ of cobalt atoms transformed into 4-fold coordination before the onset of crystallization. This is also in very good agreement with the changes in the intensity of the preedge feature where we calculate a figure of $\delta_{\mathrm{Co}}\mathrm{T_d} = 45\%$ for an intensity of 0.07. The P coordination number that increases from 1 to 2 in the meantime indicates that if we take the coordination of $\mathrm{Co_{Oh}}$ constant as 1, the $\mathrm{Co_{Td}}$ are now coordinated to at least three P atoms. In the gel 15 min before the onset of crystallization one-half of the $\mathrm{Co^{2+}}$ species are now tetrahedral and incorporated in the Al−O−P precursor units while the remaining half are still octahedral. Although these octahedral Co are connected to the aluminophosphate network by one or two bonds, they are not fully integrated.

The drop in Co−O bond distance in the second region to less than 2.04 Å is consistent with the remaining 6-fold cobalt being incorporated into the framework as tetrahedral species. This drop in the bond distance is also concurrent with a drop in the Debye−Waller factor from 0.025 to 0.005 Å^2, which reflects the lower level of disorder of $\mathrm{Co^{2+}}$ in the crystalline structure than in the gel phase. The unusual short Co−O distance of 1.90 Å adopted by $\mathrm{Co^{2+}}$ in the early stage of crystallization may indicate the presence of a proton on the oxygen shared with the P neighbor (considering the low pH of the synthesis medium, this could be possible). This short distance has indeed already been observed during the calcination of CoAPO-18 material and attributed to an intermediate protonation of the bonding O due to decomposition of the template molecules. An intermediate stage in which protons instead of template molecules are acting as balancing charge for the $\mathrm{Co^{2+}}$ may explain their temporary presence before the Co−O bond distance eventually takes its final value of 1.94 Å. However, this low average Co−O distance may also be typical for undercoordinated $\mathrm{Co^{2+}}$ species which may exist at the extern of small CoAPO-5 particles. The presence of two P shells (at 3.18 and 3.44 Å) in the crystallized material with Co−P bond distances varying accordingly with the Co−O distance indicates that some distortion of the original $\mathrm{Al^{3+}}$ site substituted by the $\mathrm{Co^{2+}}$ site has occurred through a relaxation process, which is not surprising if one considers the longer Co−O bond distance of 1.95 Å compared to the typical Al−O distance of ca. 1.72 Å.[52]

3.5. Crystallization Model. By combining the information obtained from these different techniques it is possible to derive a crystallization model for CoAPO-5 molecular sieve. From a macroscopic perspective the main property of this model is the dimensionality of crystallization. As Raman spectroscopy showed, phosphoric acid and alumina react in water instantaneously to form an Al−O−P-based gel phase. Since the Sharp−Hancock analysis of the SAXS/WAXS data for the material pointed toward a diffusion-limited 1D process, it is highly probable that the first units formed in the gel preparation could be simple 1D chains of alternating Al−O−P units. The observation of 1D structures forming from metallophosphate synthesis gels has been reported many times.[69−73] It is now generally accepted that such 1D units are formed, most probably from a series of 0D monomers (such as four-membered rings—the basic structural units of metallophosphates)[69,72,74,75] and are subsequently converted to 3D structures via a building up process or ‘Aufbau principle’. This process was initially proposed by Rao et al.[72,75] for the synthesis of zinc phosphates via the successive building up of 1D chain and ladder structures into first 2D and finally complex 3D architectures. Perhaps more significantly, the work of Oliver et al. demonstrated that all the aluminophosphate structures can be derived from the transformation of a parent single Al−O−P linear chain.[76,77] It was argued that 1D Al−O−P chains containing tetrahedral aluminum centers with terminating phosphate groups are more stable than the branched counterparts. These can easily be solvated and therefore interact with the protonated template molecule forming alkylammonium ions, which keeps them apart in solution. The cationic templates, however, are able to reduce the interchain electrostatic repulsion, allowing them to crystallize from solution. These polymeric aluminophosphate chains, which are expected to be highly flexible at elevated temperature, can undergo, through rapid rotation and bending motion, intrachain condensation leading to a porous layer or an open-framework structure. It is possible to envisage therefore that a rapid precipitation of the chains would result in an amorphous material containing layers of poorly arranged chains and that heating would cause the chains to reconstruct, cross-link, and organize to form the final crystalline structure.

Similar phenomena have been observed in zeolite synthesis.[3] With regard to a number of crystallization studies, the idea that largely covalent polymeric structures result from the aggregation of simpler building blocks seems well supported. Perhaps most relevant to this work are the studies of Kirshhock et al. on the formation of silicalite-1, where they propose a similar mechanism in which small 0D subunits aggregate together to first form chain-like ‘quarter nanoslabs’ then 2D ‘nanoslabs’ having dimensions 1.3 × 4.0 × 4.0 nm with nine intersections per particle, each of these containing a TPA cation, before aggregation of such 2D structures leads to larger particles and ultimately to the 3D crystalline MFI-type structure.[78−81] However, whether this is typical for all zeolites is still under debate.[3]

The SAXS data showed that the average particle size in the gel increased as a function of temperature from ca. 7 nm at the beginning of the reaction to ca. 20 nm just before the onset of crystallization with no change in the dimensionality of the growth process. This is in favor of a progressive condensation of chains into more highly ordered one-dimensional rodlike

---

(69) Yu, J. H.; Xu, R. R. *Acc. Chem. Res.* **2003**, *36*, 481−490.
(70) Wang, K. X.; Yu, J. H.; Song, Y.; Xu, R. R. *Dalton Trans.* **2003**, 99−103.
(71) Choudhury, A.; Neeraj, S.; Natarajan, S.; Rao, C. N. R. *J. Mater. Chem.* **2001**, *11*, 1537−1546.
(72) Ayi, A. A.; Neeraj, S.; Choudhury, A.; Natarajan, S.; Rao, C. N. R. *J. Phys. Chem. Solids* **2001**, *62*, 1481−1491.
(73) Adair, B. A.; Neeraj, S.; Cheetham, A. K. *Chem. Mater.* **2003**, *15*, 1518−1529.
(74) Ferey, G. *J. Solid State Chem.* **2000**, *152*, 37−48.
(75) Rao, C. N. R.; Natarajan, S.; Choudhury, A.; Neeraj, S.; Ayi, A. A. *Acc. Chem. Res.* **2001**, *34*, 80−87.
(76) Oliver, S.; Kuperman, A.; Lough, A.; Ozin, G. A. *Chem. Mater.* **1996**, *8*, 2391−2398.
(77) Oliver, S.; Kuperman, A.; Ozin, G. A. *Angew. Chem., Int. Ed.* **1998**, *37*, 47−62.
(78) Ravishankar, R.; Kirschhock, C. E. A.; Knops-Gerrits, P. P.; Feijen, E. J. P.; Grobet, P. J.; Vanoppen, P.; De Schryver, F. C.; Miehe, G.; Fuess, H.; Schoeman, B. J.; Jacobs, P. A.; Martens, J. A. *J. Phys. Chem. B* **1999**, *103*, 4960−4964.
(79) Kirschhock, C. E. A.; Ravishankar, R.; Verspeurt, F.; Grobet, P. J.; Jacobs, P. A.; Martens, J. A. *J. Phys. Chem. B* **1999**, *103*, 4965−4971.
(80) Kirschhock, C. E. A.; Ravishankar, R.; Jacobs, P. A.; Martens, J. A. *J. Phys. Chem. B* **1999**, *103*, 11021−11027.
(81) Kirschhock, C. E. A.; Kremer, S. P. B.; Vermant, J.; Van Tendeloo, G.; Jacobs, P. A.; Martens, J. A. *Chem.*−Eur. J. **2005**, *11*, 4306−4313.

particles that in the very last stage quickly reorganize to crystallize in the AFI structure. These precrystalline particles may be quite well organized but insufficiently so to give rise to crystalline Bragg peaks, as the material still appears to be diffraction amorphous. At 160 °C these precrystallites finally fully crystallize in the AFI structure ($<$15 min), and while crystallization proceeds, the particle size grows to ca. 40 nm. This same crystallization behavior is also observed for pure and chromium-substituted AFI[62] and can be best understood when considering the model proposed by Oliver et al. that shows that the AFI structure can be formed through intra- and interchain rearrangements of the parent chains.[77]

From an atomic perspective the evolution of the Co^{2+} local environment in the crystallization process provides further support to the observations made above. The presence of a band in the UV−vis spectrum at 470 nm and a phosphorus atom at 3.24 Å in the fit of the EXAS data revealed that octahedral Co^{2+} species such as $[CoO_4(H_2O)_2]^{2+}$ or $[CoO_5(H_2O)]^{2+}$ exist in the as-prepared gel and are attached via phosphate to the disordered Al−O−P network. However, all previous EXAS studies showed that the Co^{2+} species in the final AlPO material are tetrahedral, suggesting that a coordination state change occurs during incorporation. It is possible to envisage that such a coordination state change is necessary for incorporation because the Co−O bond distance of 2.08 Å typical of octahedral Co^{2+} is too large (much larger than the tetrahedral Al−O bond distance of ca. 1.72 Å)[52] to be incorporated into the AlPO network. This transformation apparently starts at ca. 75 °C and proceeds gradually up to 145 °C and is also accompanied by local ordering around these tetrahedral species as the increase in the number of phosphorus neighbors suggests. This change in coordination could be a direct consequence of interchain condensation of low-order Al−O−P chains resulting in Co^{2+} incorporation. This would also explain why larger particles (20 nm) are seen in the SAXS data. However, since this did not occur until a temperature of ca. 75 °C was reached, it would appear that there is an activation energy barrier which needs to be overcome before the intrachain condensation process can begin. The coordination state change is still very slow up to ca. 155 °C by which stage approximately one-half of the Co^{2+} ions have changed their coordination from 6-fold to 4-fold. On reaching the crystallization temperature (ca. 155−160 °C) all remaining Co^{2+} species are forced to adopt tetrahedral-like coordination as rapid formation of the crystalline network begins around them. Critically, it appears that adoption of tetrahedral Co^{2+} occurs before the appearance of Bragg peaks in the WAXS pattern. This may suggest that either all Co^{2+} must become tetrahedral before crystallization or formation of small particles of tetrahedral Co^{2+} containing CoAPO-5 had already begun.

Compared to pure AlPO$_4$-5 that starts to crystallize ca. 20 °C,[62] features a slightly smaller n factor ($\approx$ 1) and a crystal growth rate that is 3 times higher, it is clear that Co^{2+} plays a specific role on the more general crystallization process of the aluminophosphate network. The higher onset temperature as well as the lower rate of crystallization strongly suggested that Co^{2+} is globally slowing down the crystallization process. This is despite the amount of cobalt being as little as 2.5 wt %. The difficulty for Co^{2+} to change coordination before being incorporated into the aluminophosphate network therefore appears to hinder significantly the crystallization process of the AFI structure. However, although Co^{2+} does influence the crystallization behavior, its change of coordination reflects to a large extent the general crystallization mechanism of the AFI network. Indeed, it is noticeable that the amount of tetrahedral Co^{2+} as determined from the X-ray absorption spectroscopy data appears to be closely correlated with the extent of the condensation process as measured with the SAXS technique, showing that Co^{2+} can be used to some extent as an internal probe of the crystallization process.

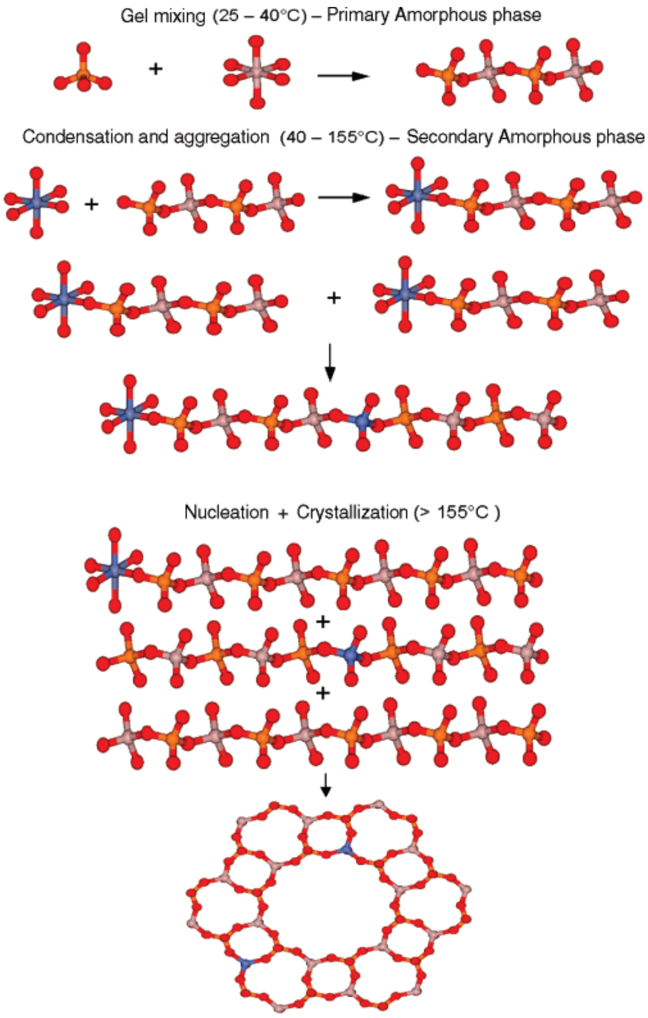

Figure 12. Schematic of the three-stage crystallization model. Note: blue = Co^{2+}, pink = Al^{3+}, orange = P^{5+}, and red = O^{2-}.

A general scheme that summarizes these different stages of the crystallization and incorporation of Co^{2+} into the aluminophosphate networks is presented in Figure 12. It is clear that combination of these in-situ techniques strongly suggests that the crystallization proceeds through a three-stage process. These three stages can be described as (i) an initial reaction of the aluminum and phosphorus reagents in a ‘primary amorphous phase’[3] from room temperature to 40 °C, (ii) aggregation of nuclei from a ‘secondary amorphous phase’ from 40 to ca. 155 °C, and (iii) nucleation and growth of the AFI structure above this temperature.

4. Conclusions

A combination of X-ray scattering and absorption techniques with UV−vis and Raman spectroscopy has proved to be a powerful method to investigate the hydrothermal synthesis of a molecular sieve, such as CoAPO-5, from both a macroscopic and an atomic perspective. The mechanism was shown to be 1D diffusion limited and can be described as a succession of stages: (i) a reaction of starting reagents to form a primary amorphous gel phase,[3] (ii) aggregation in the secondary amorphous phase from 40 to ca.155 °C, and (iii) nucleation and crystallization of the CoAPO-5 structure above this temperature. These results therefore can be best understood with reference to the chain condensation mechanism proposed by Oliver et al.[76,77] and therefore represent the first experimental evidence for such a mechanism. We note that the role of both the template molecule and the solvent is not considered in this model. However, since many different templates and a variety of solvents (both protic and aprotic) have been used to synthesize AFI and since the same template can be used to crystallize different aluminophosphate structures, we surmise that their role is not specific for AFI crystallization and therefore the mechanism proposed can be considered to be generally applicable.[82,83] The Co^{2+} ions influence the crystallization process by hindering and therefore retarding it. It is most likely that this is related to the necessity of the Co^{2+} ions to transform from octahedral into a tetrahedral geometry before being incorporated into the Al−O−P network. This slow transformation of Co^{2+} in the early stages of crystallization supports the idea obtained from the X-ray scattering data that interchain condensation is responsible for cobalt incorporation. Therefore, it can be considered that the Co^{2+} ions are acting as an internal probe of the crystallization process, and monitoring the evolution of its coordination provided us with very valuable information on the mechanism involved in this process.

Acknowledgment. Financial support from NWO-CW (VICI project) and NRSCC is kindly acknowledged. Furthermore, NWO is also thanked for granting us the beamtime at BM-26 DUBBLE (experiments 26-02-230 and 26-01-707). We wish to acknowledge the assistance and advice of Dr. Florian Meneau (DUBBLE BM26B SAXS/WAXS beamline) and Dr. Sergey Nikitenko (DUBBLE BM26A XAS beamline) during the experimental measurements. Dr. Paul Stephenson, Dr. Ian Harvey, Ad van der Eerden, and Peter de Boer are thanked for their efforts in helping to develop the QEXAFS setup on BM26A. The use of the EPSRC's Chemical Database Service at Daresbury is also gratefully acknowledged.

JA054014M

---

(82) Fan, W.; Ruifeng, L.; Dou, T.; Tatsumi, T.; Weckhuysen, B. M. *Micropor. Mesopor. Mater.* **2005**, *84*, 116−126.

(83) Szostak, R. *Molecular Sieves: Principles of Synthesis and Identification;* Van Nostrand Reinhold: New York, 1989.